

Decreased integration and information capacity in stroke measured by whole brain models of resting state activity

Mohit H. Adhikari,¹ Carl D. Hacker,² Josh S. Siegel,³ Alessandra Griffa,^{4,5} Patric Hagmann,^{4,5} Gustavo Deco^{1,6,*} and Maurizio Corbetta^{2,3,7,8,*}

*These authors contributed equally to this work.

While several studies have shown that focal lesions affect the communication between structurally normal regions of the brain, and that these changes may correlate with behavioural deficits, their impact on brain's information processing capacity is currently unknown. Here we test the hypothesis that focal lesions decrease the brain's information processing capacity, of which changes in functional connectivity may be a measurable correlate. To measure processing capacity, we turned to whole brain computational modelling to estimate the integration and segregation of information in brain networks. First, we measured functional connectivity between different brain areas with resting state functional magnetic resonance imaging in healthy subjects ($n = 26$), and subjects who had suffered a cortical stroke ($n = 36$). We then used a whole-brain network model that coupled average excitatory activities of local regions via anatomical connectivity. Model parameters were optimized in each healthy or stroke participant to maximize correlation between model and empirical functional connectivity, so that the model's effective connectivity was a veridical representation of healthy or lesioned brain networks. Subsequently, we calculated two model-based measures: 'integration', a graph theoretical measure obtained from functional connectivity, which measures the connectedness of brain networks, and 'information capacity', an information theoretical measure that cannot be obtained empirically, representative of the segregative ability of brain networks to encode distinct stimuli. We found that both measures were decreased in stroke patients, as compared to healthy controls, particularly at the level of resting-state networks. Furthermore, we found that these measures, especially information capacity, correlate with measures of behavioural impairment and the segregation of resting-state networks empirically measured. This study shows that focal lesions affect the brain's ability to represent stimuli and task states, and that information capacity measured through whole brain models is a theory-driven measure of processing capacity that could be used as a biomarker of injury for outcome prediction or target for rehabilitation intervention.

1 Center for Brain and Cognition, Computational Neuroscience Group, Department of Information and Communication Technologies, Universitat Pompeu Fabra, Ramon Trias Fargas, 25-27, Barcelona, 08005, Spain

2 Department of Bioengineering, Washington University Saint Louis, USA

3 Department of Neurology, Washington University School of Medicine Saint Louis, USA

4 Department of Radiology, Lausanne University Hospital and University of Lausanne (CHUV-UNIL), 1011 Lausanne, Switzerland

5 Signal Processing Lab 5, Ecole Polytechnique Federale de Lausanne (EPFL), 1015 Lausanne, Switzerland

6 Institutio Catalana de la Recerca I Estudis Avancats (ICREA), University of Pompeu Fabra, Passeig Lluís Companys 23, Barcelona, 08010, Spain

7 Departments of Radiology and Neuroscience, Washington University School of Medicine Saint Louis, USA

8 Department of Neuroscience, University of Padua, Italy

Correspondence to: Mohit H Adhikari
Center for Brain and Cognition, University of Pompeu Fabra,
Calle Ramon Trias Fargas, 25-27, 08005, Barcelona, Spain
E-mail: mohit.adhikari@upf.edu

Keywords: functional connectivity; information capacity; integration; whole-brain modelling

Abbreviations: DAN = dorsal attention network; DMN = default mode network; FPN = frontal parietal network; LAN = language network; RSN = resting state network; VAN = ventral attention network

Introduction

Focal brain lesions due to stroke cause behavioural impairment in different functional domains such as motor, language, attention, vision, and memory. Traditionally, these behavioural deficits are thought to originate from local dysfunction of the injured region (Scoville and Milner, 1957; Ferrier, 2012). However, since the seminal work of Von Monakow (1911; see review in Carrera and Tononi, 2014) it has been recognized that focal lesions cause physiological changes to structurally intact regions far away from the lesion, so-called ‘diaschisis’. More recently it has become apparent that focal lesions cause widespread and large-scale changes to the temporal synchronization or coherence of different brain networks, and that these changes account for behavioural variability at the acute stage (He *et al.*, 2007; Carter *et al.*, 2010; van Meer *et al.*, 2010; Wang *et al.*, 2010; Park *et al.*, 2011; Baldassarre *et al.*, 2014; reviewed in Carter *et al.*, 2012; Corbetta, 2012).

From a more theoretical perspective, network theories of brain function emphasize the importance of integration and segregation of information and neural activity in promoting efficient processing of information (Tononi *et al.*, 1994; Park and Friston, 2013). These theories have recently received strong support from computational neuroimaging studies showing that the brain’s structural and functional connectivity organization represents a trade-off between efficient processing within local modules, and metabolically expensive integration through large-scale interactions of spatially segregated modules (Bullmore and Sporns, 2009; Sporns, 2013; Deco *et al.*, 2015).

From these observations and theories follows the hypothesis that focal lesions may affect the optimal balance of integration and segregation, and that these changes may relate to large-scale abnormalities of network coherence observed empirically and potentially to behavioural deficits (He *et al.*, 2007; Andrew James *et al.*, 2009; Grefkes and Fink, 2011; Westlake and Nagarajan, 2011). To date, a few computational studies have modelled the impact of artificial lesions on network activity computed from structural models of brain connectivity (Honey and Sporns, 2008; Alstott *et al.*, 2009). However, no study has estimated the effect of focal lesions on both empirical and model-based measures of functional integration and segregation.

Here we use whole brain dynamic modelling of spontaneous (or resting state) activity to derive measures of integration and segregation in healthy subjects and patients affected by stroke. Whole brain dynamic models (Deco and Jirsa, 2012; Deco *et al.*, 2013) have been shown to reliably replicate several spatial and temporal features of functional brain networks empirically measured during rest. The models have essentially four components: (i) a realistic structural connectivity matrix (either single subject or group), obtained either using tracing studies in primates (Kötter, 2004) or diffusion spectrum/tensor imaging (DSI/DTI) in case of human brains (Hagmann *et al.*, 2008); (ii) a model of the local dynamics of neuronal activity based on intracortical recordings of real activity; (iii) a convolution of the neural activity with a model haemodynamic response; and (iv) model fitting to optimize the correlation between model and empirically measured functional connectivity.

In this study, functional connectivity was measured separately in healthy subjects and patients with stroke 2 weeks post-onset. Simulated functional connectivities were obtained by fitting the model with empirically measured functional connectivity in healthy and stroke individuals. Using the empirically-derived functional connectivity ensures that the model’s effective connectivity captures the effects of stroke on network coherence measured by functional connectivity. After model fitting, we derived a measure of ‘network integration’ and a measure of ‘network segregation’, which captures the variability of network states in response to these stimuli. Measures of integration and segregation obtained in single subject models in a group of participants with cortical stroke were compared with models in a group of age- and education-matched healthy control subjects. Further, because activations of several subnetworks called the resting state networks (RSNs) have been found by different imaging methods (Damoiseaux *et al.*, 2006; Mantini *et al.*, 2007) to be a characteristic feature of brain’s spontaneous state, and, alterations in functional connectivity-based measures at the level of RSNs have recently been shown (Baldassarre *et al.*, 2014; Siegel *et al.*, 2016) to robustly capture impact of stroke, we calculated the computational measures also at the level of seven different RSNs. We predicted that both integration and segregation measures will be decreased in stroke as compared to healthy subjects. We also examined the relationship between these model measures and empirically measured functional connectivity and behaviour.

Materials and methods

Participants

Stroke sample

Subjects ($n = 172$) were prospectively recruited, of whom 132 met post-enrolment inclusion criteria (for details see Corbetta *et al.*, 2015). Thirty-six subjects with cortical lesions were selected for this study (see ‘Selection of stroke lesions’ section below).

Inclusion criteria included: (i) age ≥ 18 with no upper age limit; (ii) first symptomatic stroke, ischaemic or haemorrhagic; (iii) up to two lacunes, clinically silent, <15 mm in size on CT scan; (iv) clinical evidence of motor, language, attention, visual, or memory deficits based on neurological examination; (v) time of enrolment: <2 weeks from stroke onset; and (vi) awake, alert, and capable of participating in research.

Exclusion criteria included: (i) previous stroke based on clinical imaging; (ii) multi-focal strokes; (iii) inability to maintain wakefulness in the course of testing; (iv) presence of other neurological, psychiatric or medical conditions that preclude active participation in research and/or may alter the interpretation of the behavioural/imaging studies (e.g. dementia, schizophrenia), or limit life expectancy to <1 year (e.g. cancer or congestive heart failure class IV); and (v) report of claustrophobia or metal object in body.

Healthy control subjects

A healthy control group ($n = 26$) were matched with the study sample for age, gender, and years of education.

Selection of stroke group based on lesions

Lesions were manually segmented on structural MRI images [T_1 , T_2 , fluid attenuated inversion recovery (FLAIR)] using the Analyze biomedical imaging software system (Robb and Hanson, 1991) and automatically classified in cortical, subcortical, and cortico-subcortical based on their overlap with three masks (grey matter, white matter, and subcortical regions including basal ganglia and thalamus). Each mask was computed as 50% conjunction of 38 single subject FreeSurfer (<http://surfer.nmr.mgh.harvard.edu/>) (Dale *et al.*, 1999) grey and white matter segmentations obtained from an independent group of healthy volunteers (age range = 18–35) on $1 \times 1 \times 1$ mm MP-RAGE T_1 -weighted images. A K-means clustering in MatLab (MatLab Works) was run using the per cent of lesion volume that intersected with each mask (i.e. number voxels in the lesion overlapping with each mask/total number of voxels in the lesion) as input, to display the overlap of each lesion group with grey matter, white matter, and subcortical nuclei. The number of lacunes on the MRI was recorded and the periventricular white matter was rated according to Longstreth *et al.* (1996). The group of ‘cortical’ lesions ($n = 36$) were selected for this study. This makes it more likely that the effect on functional connectivity is due to damage of cortical nodes, which is how the model is organized.

Functional MRI

Procedure and scanning

Scanning was performed with a Siemens 3 T Tim-Trio scanner at the School of Medicine of the Washington University in St. Louis. Patients underwent a scanning session within 2 weeks (mean = 13.4 days, SD = 4.8 days) after the stroke. All participants underwent structural, functional and diffusion tensor scans. Structural scans consisted of: (i) a sagittal MP-RAGE T_1 -weighted image (repetition time = 1950 ms, echo time = 2.26 ms, flip angle = 90° , voxel size = $1.0 \times 1.0 \times 1.0$ mm, slice thickness = 1.00 mm); (ii) a transverse turbo spin-echo T_2 -weighted image (repetition time = 2500 ms, echo time = 435 ms, voxel-size = $1.0 \times 1.0 \times 1.0$ mm, slice thickness = 1.00 mm); and (iii) a sagittal FLAIR (repetition time = 7500 ms, echo time = 326 ms, voxel-size = $1.5 \times 1.5 \times 1.5$ mm, slice thickness = 1.50 mm). PASL acquisition parameters were: repetition time = 2600 ms, echo time = 13 ms, flip angle = 90° , bandwidth 2.232 kHz/pixel, and field of view = 220 mm; 120 volumes were acquired (322 s total), each containing 15 slices with slice thickness 6- and 23.7-mm gap. Resting state functional scans were acquired with a gradient echo EPI sequence (repetition time = 2000 ms, echo time = 27 ms, 32 contiguous 4-mm slices, 4×4 mm in-plane resolution) during which participants were instructed to fixate on a small cross in a low luminance environment. Six to eight resting state functional MRI runs, each including 128 volumes (30 min total), were acquired.

Data preprocessing

Functional MRI data underwent a preprocessing procedure consisting of the following steps: (i) asynchronous slice acquisition was compensated by sinc interpolation to align all slices; (ii) elimination of odd/even slice intensity differences resulting from interleaved acquisition; (iii) a whole brain normalization corrected for changes in signal intensity across scans; (iv) data were realigned within and across scans to correct for head movement; and (v) EPI data were co-registered to the subject's T_2 -weighted anatomical image, which in turn was co-registered with the T_1 -weighted MP-RAGE, in both cases using a cross-modal procedure based on alignment of image gradients (Rowland *et al.*, 2005). The MP-RAGE was then transformed to an atlas-space (Talairach and Tournoux, 1988) representative target using a 12-parameter affine transformation. Movement correction and atlas transformation were accomplished in one resampling step (resulting in an isotropic 3 mm voxel size) to minimize blur and noise. In preparation for the functional connectivity MRI analysis, data were passed through several additional preprocessing steps (Fox *et al.*, 2005): (i) spatial smoothing (6 mm full-width at half-maximum Gaussian blur); (ii) temporal filtering retaining frequencies in the 0.009–0.08 Hz band; and (iii) removal of the following sources of spurious variance unlikely to reflect spatially specific functional correlations through linear regression: (a) six parameters obtained by rigid body correction of head motion; (b) the whole-brain signal averaged over a fixed region in atlas space; (c) signal from a ventricular region of interest; and (d) signal from a region centered in the white matter.

The decision to include whole-brain signal as a nuisance regressor was made in light of numerous studies showing that whole-brain signal regression removes substantial

confound attributable to head motion and respiration (CO₂) and reduces spurious correlations in blood oxygen level-dependent (BOLD) data (Power *et al.*, 2012, 2015; Satterthwaite *et al.*, 2012; Van Dijk *et al.*, 2012). A recently published report found that functional connectivity changes observed in stroke patients relative to age-matched controls were consistent with and without whole brain signal regression (Siegel *et al.*, 2016).

Quality control of resting state data

For each frame of resting state functional MRI scans a DVARS (temporal derivative of time courses of root mean square variance over voxels) score was calculated. DVARS indexes the rate of change of the BOLD signal across the entire brain at each frame of data; the rationale and method for calculating DVARS has been described previously (Power *et al.*, 2012). To define the DVARS threshold for our group of patients, we computed the mean plus 2 standard deviation (SD) of DVARS values for all frames, excluding the first four frames, in the group of age-matched control subjects. The threshold was equal to 4.6. All frames in the resting state functional MRI scans with a DVARS value of ≥ 4.6 were removed from the analysis. After frame censorings, patients retained 788 ± 94 (mean \pm SD) frames out of 878 ± 69 frames acquired. Controls retained 732 ± 154 frames out of 872 ± 100 frames acquired.

Behavioural testing

All subjects and controls underwent a behavioural battery that included assessment of motor, language, attention, memory, and visual function following each scanning session. Overall clinical deficit was also assessed in each patient using the NIH stroke scale (NIHSS) (Brott *et al.*, 1989). Imaging and behavioural testing session usually were performed on the same day. Dimensionality reduction was performed on the behavioural performance data as described previously (Corbetta *et al.*, 2015). Principal components analysis was performed on all tests within a behavioural domain to produce a single score that predicted the majority of variance across tasks. The ‘Motor’ score describes contralesional deficits that correlated across shoulder flexion, wrist extension/flexion, ankle flexion, hand dynamometer, nine hole peg, action research arm test, timed walk, functional independence measure, and the lower extremity motricity index. The ‘Attention (visual field)’ score describes contralesional visual field effects in Posner, Mesulam, and BIT centre of cancellation tasks. A separate ‘Attention (sustained)’ score loaded on non-spatial measures of overall performance, reaction time, and accuracy on the same tests. The ‘Spatial Memory’ score loaded on the Brief Visuospatial Memory Test and spatial span. The ‘Verbal Memory’ score loaded on the Hopkins Verbal Learning Test. The ‘Language’ score loaded on both comprehension (complex ideational material, commands, reading comprehension) and production (Boston naming, oral reading).

Structural connectivity

Neuroanatomical structural connectivity was obtained using diffusion spectrum imaging (DSI) data and tractography from a different cohort of 10 healthy right-handed male subjects. DSI and MP-RAGE T₁-weighted acquisitions were performed

on a Siemens 3.0 T TIM Trio MRI scanner (Siemens Healthcare) equipped with a 32-channel head coil. The DSI sequence included 128 diffusion-weighted images with a maximum b-value of 8000 s/mm² and one b0 reference image. The acquisition volume comprised $96 \times 96 \times 34$ voxels with $2.2 \times 2.2 \times 3$ mm resolution. Repetition and echo times were 6100 and 144 ms, respectively. The MP-RAGE acquisition had a 1 mm in-plane resolution and 1.2 mm slice thickness, covering $240 \times 257 \times 160$ voxels. Repetition, echo and inversion times were 2300, 2.98 and 900 ms, respectively.

The grey matter was parcellated in 34 cortical areas per hemisphere (68 areas in total) according to anatomical landmarks (Desikan *et al.*, 2006). This was followed by a further parcellation into 1000 regions of interest of approximately equal areas (number of voxels) (Cammoun *et al.*, 2012). Deterministic streamline tractography within the white matter was used to estimate the fibre tract density connecting each pair of regions of interest. Anatomical connectivity strength between every pair of regions of interest was calculated by dividing the number of connecting fibres by the average area of the two regions of interest and by average fibre length between the two regions of interest (Hagmann *et al.*, 2008).

Parcel assignment to resting state networks

Grey matter parcels were assigned to resting state networks for several purposes: ordering matrices for visual display (Fig. 3), to compute RSN-averaged statistics for integration (Fig. 5), information capacity (Fig. 6), and to summarize the relationship between computational measures and functional MRI correlations (Fig. 7). Seven RSNs, namely, the dorsal attention network (DAN), ventral attention network (VAN), motor network (MOT), visual network (VIS), frontal parietal network (FPN), language network (LAN) and default mode network (DMN), were derived from a meta-analysis of task-based functional MRI studies (described in Hacker *et al.*, 2013). This work provided a population level description of the cortical surface distribution of RSNs by computing an averaging across individually estimated RSN topographies in 692 subjects. The group-average RSN estimate was sampled using the surface parcels in the present study. Each parcel was assigned in a winner-take-all fashion to the RSN with the greatest estimate (i.e. the RSN with the highest score after averaging over all vertices within the parcel). Details on quantification and interpretation of RSN membership estimates for individual brain loci in single subjects are described in Hacker *et al.* (2013).

Dynamic mean field model

The model is an approximation of a spiking network model (Deco and Jirsa, 2012) consisting of populations of excitatory and inhibitory neurons and it expresses the averaged activity of each population using a single variable, namely the average firing rate. Inter-area connections between the excitatory pools were weighted by the structural connectivity matrix and a global scaling factor, G . As the global scaling factor was varied, the local feedback inhibition was adjusted to constrain the average firing rate of each local excitatory population. For complete description of model equations and parameters refer to Deco *et al.* (2014)*b*. Model equations were simulated for

10 min to obtain neuronal activity of each brain area. We then transformed it to BOLD signal using the Balloon-Windkessel haemodynamic model (Friston *et al.*, 2003). Finally, we calculated the simulated functional connectivity using correlation between simulated BOLD signals of all brain area-pairs.

Effective connectivity

First the network model, in which dynamic mean field models for local areas were coupled using structural connectivity averaged across 10 healthy subjects, was simulated for several values of the global scaling factor G . Resulting simulated functional connectivities were compared with empirical functional connectivity for every subject using Pearson correlation (Deco *et al.*, 2014b). As Supplementary Fig. 8A and B display, these correlations for both control and stroke subjects as a function of G increase and saturate beyond $G \approx 4.0$ for all subjects. Therefore, we fixed the value G at 4.0 in all future simulations for all subjects. We then used a gradient descent algorithm (Deco *et al.*, 2014a) to adjust (i) all interhemispheric homotopic connections; and (ii) any other pairwise connections that were stronger than 0.5% of the strongest connection in the average structural connectivity matrix we had to obtain an optimal correlation between the empirical functional connectivity and the simulated functional connectivity. This number amounted to 18% of total connections. The optimizing procedure involved the following steps:

- (i) In the first step, we used the original structural connectivity and $G (=4.0)$ in the dynamic mean field model to obtain the simulated time-series for each area.
- (ii) Subsequently, we calculated the simulated functional connectivity between all area-pairs and variance for each area and calculated the Pearson correlation between simulated functional connectivity and the empirical functional connectivity.
- (iii) We then updated the strengths (C_{ij}) of only connections mentioned above using the equation:

$$C_{ij} = C_{ij} + gV * C_{ij} * (eVi - sVi) + gFC * (eFC_{ij} - sFC_{ij}) \quad (1)$$

where eVi and sVi are the empirical and simulated variances respectively, of area i ; eFC_{ij} and sFC_{ij} are the empirical and simulated functional connectivity of brain area pair ij . gV and gFC are the gain parameters, which are set to 0.01 and 0.015, respectively. If C_{ij} became negative, we set it to zero.

- (iv) We then used this updated structural connectivity matrix and repeated the first three steps for 30 iterations.

As Supplementary Fig. 1A and B shows, the Pearson correlation between the model and empirical functional connectivity increases with each iteration and saturates after about 10 iterations for most subjects. Therefore, we choose the updated structural connectivity matrix and the corresponding functional connectivity matrix at the 10th iteration as optimal ones. Finally, as the dynamic mean field model is a stochastic model, we repeated this entire procedure for every subject 10 times and took the average of the optimal structural and functional connectivity matrices across these repetitions to obtain the final effective connectivity and model functional connectivity.

Model-based measures

Information capacity

Information capacity measures the response of the large-scale network to different stimuli (Deco *et al.*, 2015). This measure was calculated for each healthy subject and stroke patient by inserting the corresponding effective connectivity in the dynamic mean field model and simulating it. An external input $I_{external} = 0.02$ nA was applied to the excitatory population of 10% of the brain areas, randomly selected. The procedure was repeated for 1000 trials and the resulting evoked responses of the network were binarized by imposing a threshold. The threshold is a multiple of the standard deviation in the values of the evoked responses of all areas across all 1000 trials. Next, of the 1000 resulting binarized patterns, the null patterns in each of which the activity of all brain areas was below the threshold were discarded. The entropy of the remaining R non-null, evoked binary patterns is defined as:

$$H(R) = - \sum_{i=1}^n p_i \log_2 p_i \quad (2)$$

where n is the number of unique patterns and p_i is the probability that pattern i is observed. The information capacity is the normalized entropy, which is obtained by dividing $H(R)$ by its maximum value ($H_{max} = \log_2 R$) (Deco *et al.*, 2014b). To remove the sampling bias, we corrected the entropy values by using a quadratic extrapolation procedure (Treves and Panzeri, 1995).

In the case of stroke subjects, we decreased the evoked responses of all damaged brain areas in proportion to the damage suffered by them before applying the threshold. This was done primarily for mathematical considerations as our mean field model considers an average of activity of individual excitatory neurons in each local brain area and we assumed that the damage suffered by each region of interest results in the death of neurons, thereby decreasing the average activity or response. To our knowledge, the precise relationship between the extent of damage of a region of interest and its average activity (in terms of mean firing rate) is not described in the literature.

To compare the information capacity values across subjects, it was necessary to have identical number of non-null patterns for each case as otherwise, higher number of non-null patterns typically yielded higher value of entropy. This condition required us to calculate a precise value of the threshold for binarization in the case of each subject.

Integration measure

The integration measure is a graph theoretical measure found from the empirical and optimal simulated functional connectivity matrix (Deco *et al.*, 2015). For a given absolute threshold, θ , between 0 and 1, the functional connectivity is binarized (using the criterion $|FC_{ij}| < \theta$ which determines whether the ij^{th} connection will be 0 or 1). We then find the largest connected component (a subnetwork or subgraph), in which any two nodes are connected to each other by paths and not connected to any nodes outside the component, and calculate its size in terms of number of nodes. We calculate this size (normalized by the total number of areas in the network) for a range of thresholds between 0 and 1 and obtain a curve

as shown in Fig. 2C. The integration measure is the area under this curve.

Empirical functional connectivity-based measures

Homotopic functional connectivity

Averaged functional connectivity for all pairwise connections between (i) all interhemispheric homotopic brain areas; (ii) all interhemispheric homotopic brain areas belonging to each RSN; and (iii) averaged across RSNs.

Inter-resting state network functional connectivity

Average functional connectivity between all brain areas belonging to ‘extrinsic’ networks such as the DAN, VAN, motor network and visual network, and those belonging to ‘intrinsic’ networks such as DMN, FPN and LAN within the lesioned hemisphere.

Statistical tests

All correlations between the computational measures defined in this study and empirically measured characteristics such as functional connectivity-based measures, behavioural scores, lesion volume and network properties of structural connectivity were obtained using Pearson correlation. All comparisons of averages between group of healthy participants and participants with stroke were done using unpaired *t*-test. We corrected for multiple comparisons using Benjamini-Hochberg procedure for controlling false discovery rate (Benjamini and Hochberg, 1995).

Results

Subjects with stroke ($n = 36$) were enrolled prospectively based on the occurrence of a first time stroke and persistence of neurological impairment at the time of the discharge from the stroke unit. For inclusion and exclusion criteria, see the ‘Materials and methods’ section. This sample is part of a larger cohort of $n = 132$ patients described fully in Corbetta *et al.* (2015). We selected for this study only patients with predominantly cortical lesions to insure that the lesions directly damaged the nodes of the computational model, which is based on a cortical parcellation. Controls ($n = 26$) were selected to be demographically matched to patients. No significant difference was found between patients and controls in number of R-functional MRI frames (*t*-statistic = 1.78, $P = 0.079$) or head motion (*t*-statistic = -1.03 , $P = 0.31$).

Table 1 shows the clinical characteristics of the sample. This group of patients was heterogenous in lesion location and impairment by design in the experiment. Figure 1 shows the frequency distribution of lesions mapped onto a normalized cortical surface in atlas space. The most frequently damaged regions were the left inferior parietal lobule, right inferior frontal gyrus, right lateral occipital, and precentral cortex. Behaviourally, patients showed

significantly worse scores on language, spatial attention, verbal memory, and motor tasks.

Figure 2 displays the whole brain computational modelling and measures used in this study. The model functional connectivity matrix obtained by computing the pairwise temporal correlation across all regions of interest after convolving the model neural data with a haemodynamic response function was optimized at the individual subject level to match the empirically measured functional connectivity matrix both in healthy and stroke participants.

Figure 3A–F displays the effective connectivity, model functional connectivity and empirical functional connectivity for a single healthy subject (stroke patient). Supplementary Fig. 2 displays these matrices, averaged across the two groups. The brain regions in each matrix are ordered according to their assignment to seven RSNs as in Hacker *et al.* (2013). In the healthy empirical functional connectivity there is a considerable correlation among brain regions that belong to the same RSN. This modularity is considerably attenuated in the stroke patients. The correlation between model and empirical functional connectivity was close to $r = 0.75$ in both healthy and stroke groups except for two healthy subjects who were removed from further analyses (Fig. 3G).

The effective connectivity in the model reflected the amount of damage produced by the lesion, which was expressed as the fraction of damaged vertices belonging to each brain region. When comparing the fraction of damaged vertices across all regions with at least 1% damage, we found that it was positively correlated with the fractional decrease of those regions’ effective connectivity ($r = 0.3$, $P = 4 \times 10^{-6}$) (Fig. 3H).

As the effective connectivity procedure optimizes several parameters, we trained the algorithm, for each participant, using functional connectivity calculated from half the data points and validating it against the functional connectivity calculated using the other half. Supplementary Fig. 3 displays the Pearson correlation between model functional connectivity and empirical functional connectivity, for each participant, for the training set (Supplementary Fig. 3A and B) and for the validation set (Supplementary Fig. 3C and D) as a function of learning iterations. Mean correlation between model functional connectivity and empirical functional connectivity for the training and validation dataset was found to be 0.65 and 0.58, respectively, for the healthy group and 0.63 and 0.55, respectively, for the stroke group.

Having optimized the whole brain dynamic model, we examined measures of integration and segregation. First, we calculated the integration measure from both empirical functional connectivity and model functional connectivity for each of 24 control and 36 stroke participants. Both mean model and empirical integration values were lower in the stroke group, with a significant difference in the model values as compared to healthy controls (Fig. 4A and B).

Table 1 Clinical characteristics of cortical stroke sample

ID	Age	Gender	Stroke type	Side	Territory	Volume (mm ³)	tPA	NIHSS	Information capacity	Integration
029	50	Male	Ischaemic	Left	MCA	776	0	2	0.86	0.54
030	50	Female	Ischaemic	Right	MCA	5332	0	10	0.87	0.38
033	56	Female	Ischaemic	Left	MCA	910	0	6	0.85	0.53
035	59	Female	Ischaemic	Left	PCA	2462	0	2	0.86	0.49
041	63	Male	Ischaemic	Left	ACA	4161	0	12	0.61	0.66
056	52	Male	Ischaemic	Right	MCA	1399	0	3	0.87	0.57
063	45	Female	Ischaemic	Left	MCA	5177	0	7	0.80	0.50
064	55	Male	Ischaemic	Left	ACA	1164	0	1	0.86	0.56
072	63	Female	Ischaemic	Right	MCA	10186	0	10	0.88	0.50
073	43	Female	Ischaemic	Right	PCA	2275	0	1	0.91	0.53
074	47	Male	Ischaemic	Right	PCA	146	0	2	0.89	0.50
078	62	Male	Ischaemic	Left	ACA	991	0	–	0.77	0.49
082	61	Female	Ischaemic	Right	MCA	5906	0	2	0.85	0.47
083	60	Male	Ischaemic	Left	PCA	336	0	1	0.90	0.32
084	51	Female	Ischaemic	Right	PCA	323	0	1	0.89	0.49
085	72	Female	Ischaemic	Left	MCA	584	0	1	0.26	0.63
087	57	Male	Ischaemic	Right	MCA	2565	0	2	0.78	0.55
092	66	Male	Ischaemic	Left	MCA	470	0	4	0.87	0.52
097	44	Male	Ischaemic	Left	MCA	771	0	6	0.83	0.57
108	70	Female	Ischaemic	Left	MCA	6287	0	4	0.90	0.49
114	53	Female	Ischaemic	Right	PCA	7920	0	4	0.18	0.59
115	58	Male	Haemorrhagic conversion	Left	MCA	7104	0	6	0.74	0.53
116	54	Female	Ischaemic	Right	MCA	313	0	2	0.78	0.55
119	61	Female	Ischaemic	Left	MCA	3911	0	–	0.90	0.56
120	77	Male	Ischaemic	Left	PCA	2833	0	–	0.91	0.33
122	64	Male	Ischaemic	Left	MCA	6975	0	8	0.21	0.63
124	41	Male	Ischaemic	Left	PCA	324	0	0	0.84	0.42
133	62	Male	Ischaemic	Right	MCA	9475	0	10	0.78	0.52
136	49	Male	Ischaemic	Left	PCA	362	0	0	0.61	0.53
144	43	Female	Ischaemic	Left	MCA	2714	0	13	0.81	0.56
163	45	Female	Ischaemic	Left	PCA	1222	0	0	0.67	0.60
164	47	Female	Carotid dissection	Right	MCA	3650	0	1	0.73	0.51
165	52	Male	Ischaemic	Right	PCA	255	0	1	0.91	0.42
166	60	Male	Ischaemic	Right	PCA	2657	0	3	0.85	0.55
168	50	Male	Ischaemic	Left	MCA	179	0	1	0.90	0.55
196	50	Male	Ischaemic	Left	MCA	867	0	0	0.82	0.55
Mean	55.33	20 male/16 female	–	22 left/14 right	–	2861	–	3.82	0.78	0.52
SD	8.75	–	–	–	–	2861	–	3.75	0.19	0.07

NIHSS scores were acquired during the initial clinical visit within 48 h of the stroke. tPA = tissue plasminogen activator.

Second, we calculated information capacity in each subject, for nine different numbers of non-null patterns and compared group averages for each case. As shown in Fig. 4C, mean information capacity was lower in stroke than healthy subjects for all nine cases; however, the difference was not statistically significant in any of them or when averaged across all cases (Fig. 4D). The information capacity values for all cases displayed strong pairwise correlations (Supplementary Fig. 4).

We found no significant correlation between information capacity and integration values with total lesion volume (Fig. 4E and F). There was a significantly negative correlation ($r = -0.35$; $P = 0.04$) between integration and mean betweenness centrality of lesioned cortex, but no

correlation between centrality measures and information capacity (Supplementary Fig. 5). Values of integration and information capacity were not correlated (Fig. 4G), suggesting that these measures evaluate two independent properties of the underlying brain network.

Next, we calculated these measures for each of the seven RSNs described in the methods. Model integration was significantly lower in stroke as compared to healthy controls for every RSN, as well as when averaged across all RSNs (Fig. 5). Empirical integration was significantly reduced in stroke patients for all RSNs except VAN and LAN (Supplementary Fig. 6). The information capacity, calculated for 500 non-null patterns, was also significantly lower in stroke patients in DAN, FPN and when averaged

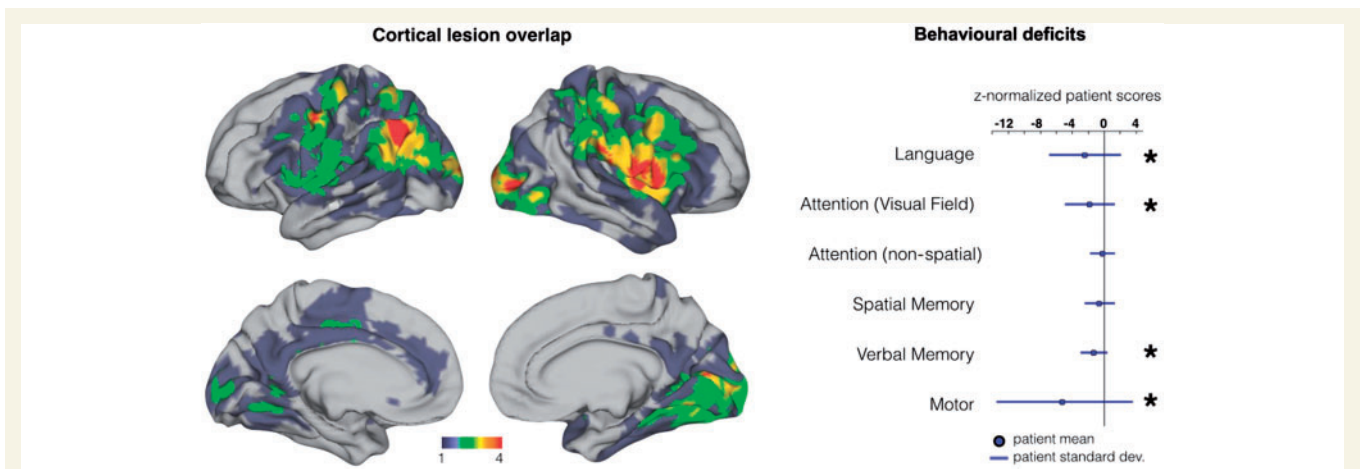


Figure 1 Lesion and behavioural data. *Left:* Surface lesion conjunction map for 36 cortical stroke patients. *Right:* Deficit in six behavioural domains for patients ($n = 36$) relative to age-matched controls ($n = 26$). In each behavioural domain, a single factor score was determined for each patient and control based on multiple behavioural tests. Scores are z-normalized based on aged-matched controls (control mean = 0 and SD = 1). Domains in which the patients differ significantly from controls are indicated with an asterisk ($P < 0.05$ after correction for six comparisons).

across all RSNs (Fig. 6). Differences in group means in all these comparisons were significant at the 0.05 level after correcting for multiple comparisons using Benjamini-Hochberg procedure for controlling false discovery rate.

An important question for the interpretation of these measures of network integration and information capacity is their relationship with empirically measured functional connectivity changes at the level of networks, which in turn correlate with behavioural impairments in different domains (motor, attention, language, etc.) (He *et al.*, 2007; Carter *et al.*, 2010; Baldassarre *et al.*, 2014). We specifically focused on two measures—the homotopic functional connectivity and the inter-RSN functional connectivity as described in the ‘Materials and methods’ section. In our sample the average homotopic functional connectivity was significantly reduced in stroke subjects, but there was no significant difference in inter-RSN functional connectivity (Fig. 7A and B). Further, the homotopic functional connectivity was less strongly related to information capacity than integration (Fig. 7C and D). While homotopic functional connectivity values only in the motor, FPN and LAN were significantly correlated with motor information capacity, its values for all RSNs except VAN correlated significantly with model integration in most RSNs, as well as for the whole brain. These relationships were found to be significant at the 0.05 level after correcting for multiple comparisons using Benjamini-Hochberg procedure.

By contrast, information capacity was more related to the segregation of RSNs within the lesioned hemisphere (Supplementary Fig. 7). While model integration was not correlated with inter-RSN functional connectivity values, global information capacity values were significantly negatively correlated with them ($r = -0.42$, $P = 0.01$) as well as with inter DAN-DMN functional connectivity values ($r = -0.4$, $P = 0.015$). The DAN and DMN are two

networks that are frequently negatively correlated during high performance even in healthy subjects (Kelly *et al.*, 2008; Sestieri *et al.*, 2010) and that represent the pivot networks of the two large extrinsic and intrinsic systems of RSNs noted above.

Finally, we compared integration and segregation measures with behavioural deficits in stroke patients. These behavioural deficits were measured in terms of factor scores in four domains (Corbetta *et al.*, 2015) – language (Lang), motor function, coded by side of the body contralateral versus ipsilateral to the stroke (MotIC), visuospatial attention coded by lateralized performance to contralateral versus ipsilateral visual stimuli (AttVFIC), attention performance overall (AttAVE) indexing accuracy and speed of processing independently of the side of the stimulus, spatial and verbal memory (MemS and MemV).

Non-zero values in Fig. 7E and F display the correlations between computational measures and behavioural factor scores that were found to be significant ($P < 0.05$, non-parametric permutation test). Information capacity values for the FPN positively correlated with language and spatial memory factor score (Fig. 7E). Specifically, high information capacity in the DMN was correlated with high overall performance, i.e. faster reaction time and more accurate visual discrimination. Integration values for the DAN and FPN correlated positively with visuospatial attention scores (AttnVFIC) (Fig. 7F). None of these relationships were found to be significant at 0.05 level when corrected for multiple comparisons using Benjamini-Hochberg procedure for controlling false discovery rate. Therefore, we fitted a multiple linear regression model using the values of information capacity for DMN and FPN and global integration values as predictors for each of the behavioural factor scores. We found information capacity for FPN to be a significant predictor for language (beta = 16.6; $P = 0.01$) and spatial

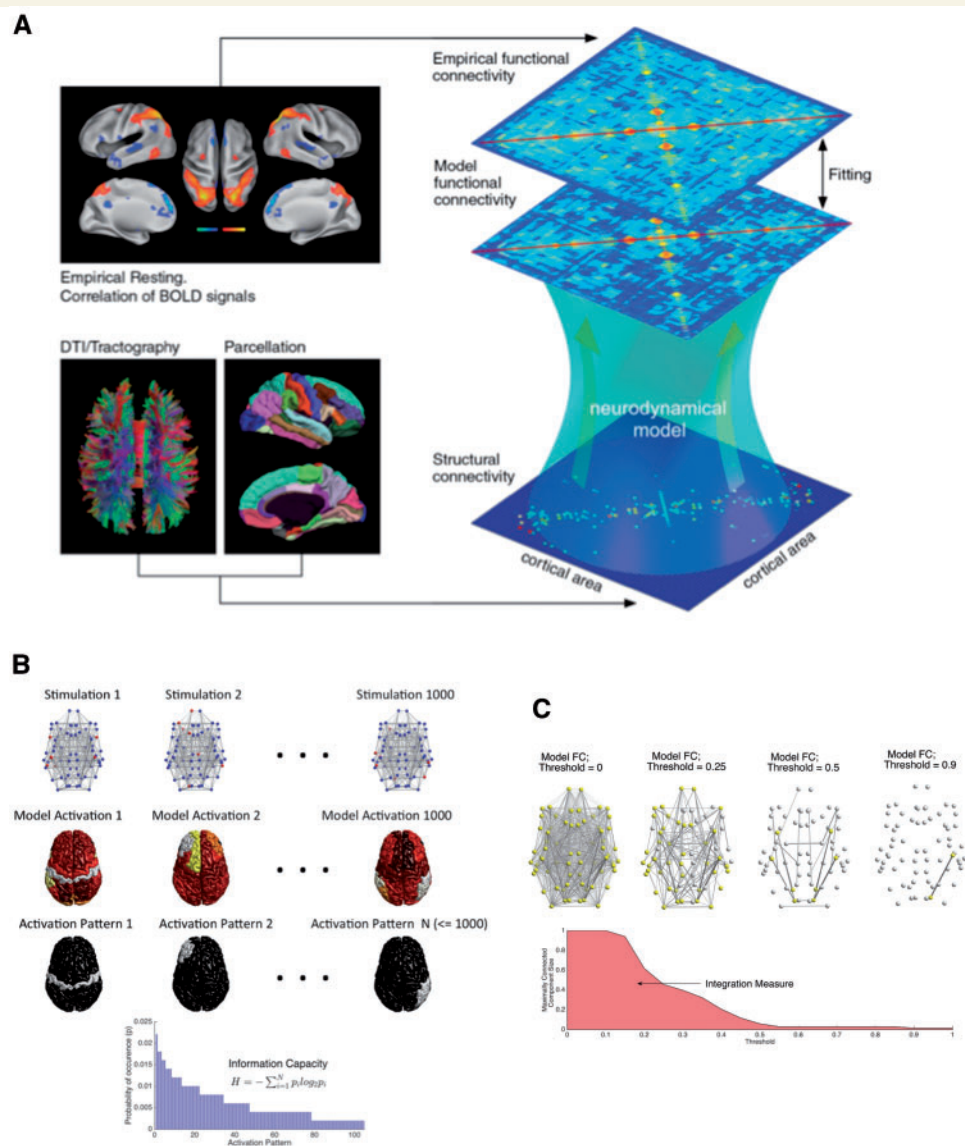


Figure 2 Methodology and description of measures. (A) General methodology used in this study (from Deco et al., 2014b). The empirical functional connectivity is obtained as correlations between BOLD signals from 68 brain areas for each healthy subject and for each subject with stroke. The model functional connectivity is found by simulating a network model consisting of a mathematical model for each brain area and an effective connectivity between brain areas. (B and C) Procedures to calculate the computational measures used in this study. (B) For information capacity, we applied an external stimulus to 10% of the network nodes (in red, top) chosen randomly and simulate the model using the effective connectivity matrix for each subject to obtain simulated BOLD activations (middle) of all brain areas. Subsequently, we apply a threshold to obtain a binary activation pattern (bottom) and repeat the process 1000 times. The information capacity is an entropy measure based on the frequency of occurrence of distinct, non-zero activation patterns. (C) The integration measure is obtained by finding the largest connected component (in yellow) from the optimized model functional connectivity (FC) at varying thresholds and by integrating its size over the range of thresholds.

memory ($\beta = 26.5$; $P = 0.002$) factor scores while information capacity for DMN was a significant predictor for overall attention performance ($\beta = 5.9$, $P = 0.03$).

Discussion

In this study, we sought to characterize the impact of stroke on measures of network segregation and integration

obtained using an *in silico* whole brain dynamic computational model of brain activity derived from functional MRI data measured in the resting state. The integration measure is related to the level of connectedness of the underlying network whereas the information capacity refers to the network's ability to encode distinct stimuli in distinct activity patterns. If the network is completely uncorrelated (segregated), the patterns of response to topographically distinct patterns of stimuli are completely distinct and information

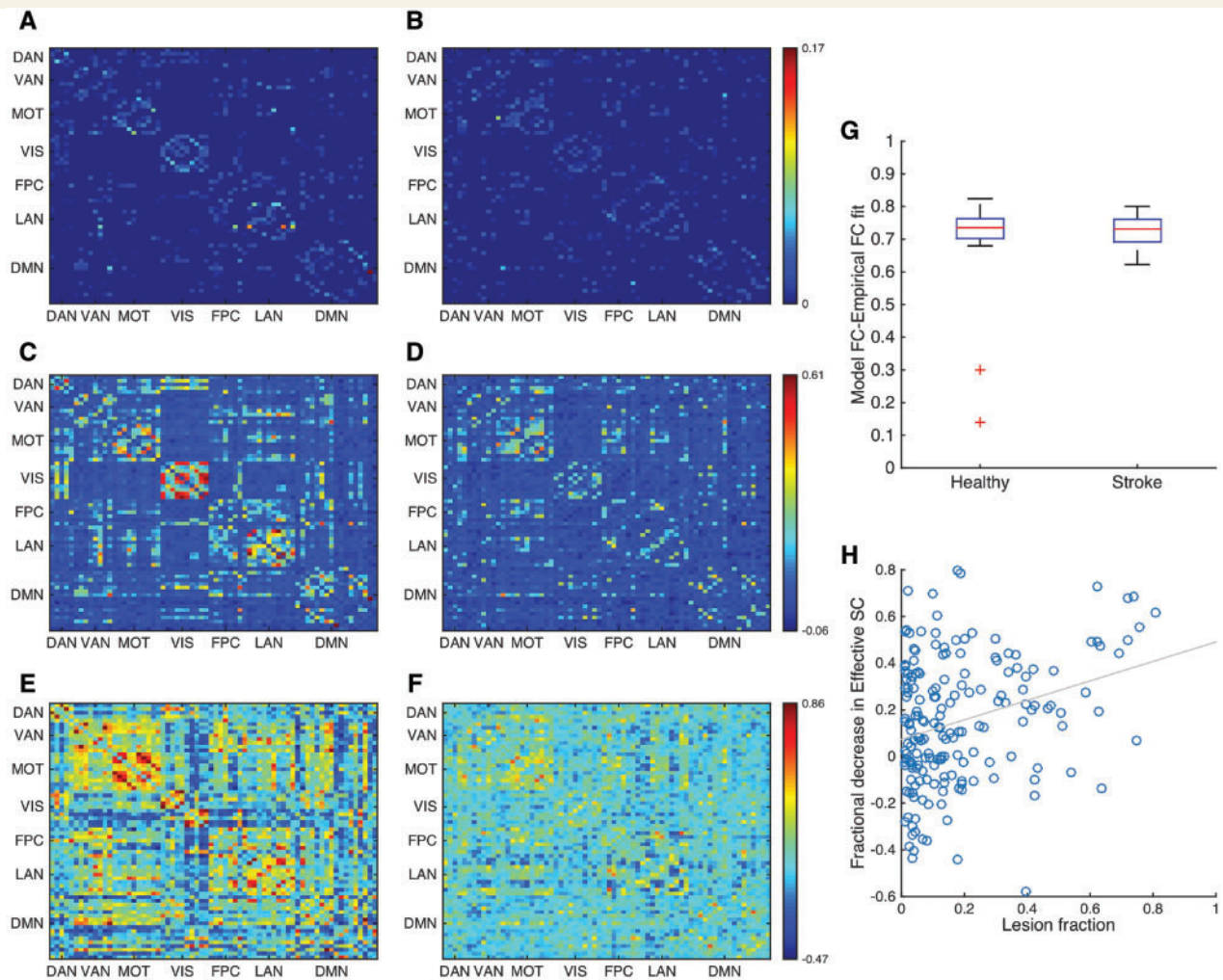


Figure 3 Model functional connectivities from effective connectivity. (A and B) Effective connectivities calculated using the network model and the empirical functional connectivity (FC) for a single healthy subject (A) and that of a subject with stroke (B). (C and D) Optimized model functional connectivities for the healthy subject (C) and that of the subject with stroke (D). (E and F) Empirical functional connectivity for the healthy subject (E) and that of the subject with stroke (F). Each matrix is ordered according to the parcels assigned to different RSNs. Reduced within-RSN connectivity in the case of stroke is observed in empirical functional connectivity of stroke subject in comparison with the healthy case, and is captured by the effective connectivity and the corresponding model functional connectivity. (G) Box plot of optimum correlation between model functional connectivity and empirical functional connectivity for all healthy subjects and stroke patients. Barring two healthy subjects, which are not considered for further analysis, the effective connectivity yields a median correlation of ~ 0.75 for both groups. (H) The lesion fraction (measured in terms of fraction of vertices damaged) of lesioned brain areas from all subjects displays significant correlation with the corresponding decrease in their effective connectivity ($r = 0.3$, $P = 4 \times 10^{-6}$). MOT = motor network; SC = structural connectivity; VIS = visual network.

capacity is maximum. On the other hand, if the network is completely correlated, all areas are activated irrespective of distinct topography of stimuli patterns, hence the variability of responses and the information capacity is zero. In this sense, the information capacity is a measure of segregation. We obtained these measures using the resting state functional MRI data from 24 healthy subjects and 36 first-time stroke patients with only cortical lesions. These data were obtained at the subacute phase upon the onset of stroke (2 weeks post-onset).

We found a significantly diminished whole-brain ability for functional integration in stroke patients in comparison with

their age-matched healthy subjects. Information capacity was also decreased in stroke patients, but the difference was not statistically significant when calculated using the entire brain network. When we calculated these measures by dividing all brain regions into seven RSNs, the mean integration was significantly lower in stroke than healthy subjects for each RSN and for the average across RSNs. Similarly, differences in information capacity were also stronger at the network level, with two of seven RSNs and their average showing significantly lower values in stroke. Differences in integration and information capacity in stroke were not related to lesion volume. These model measures correlated with the most

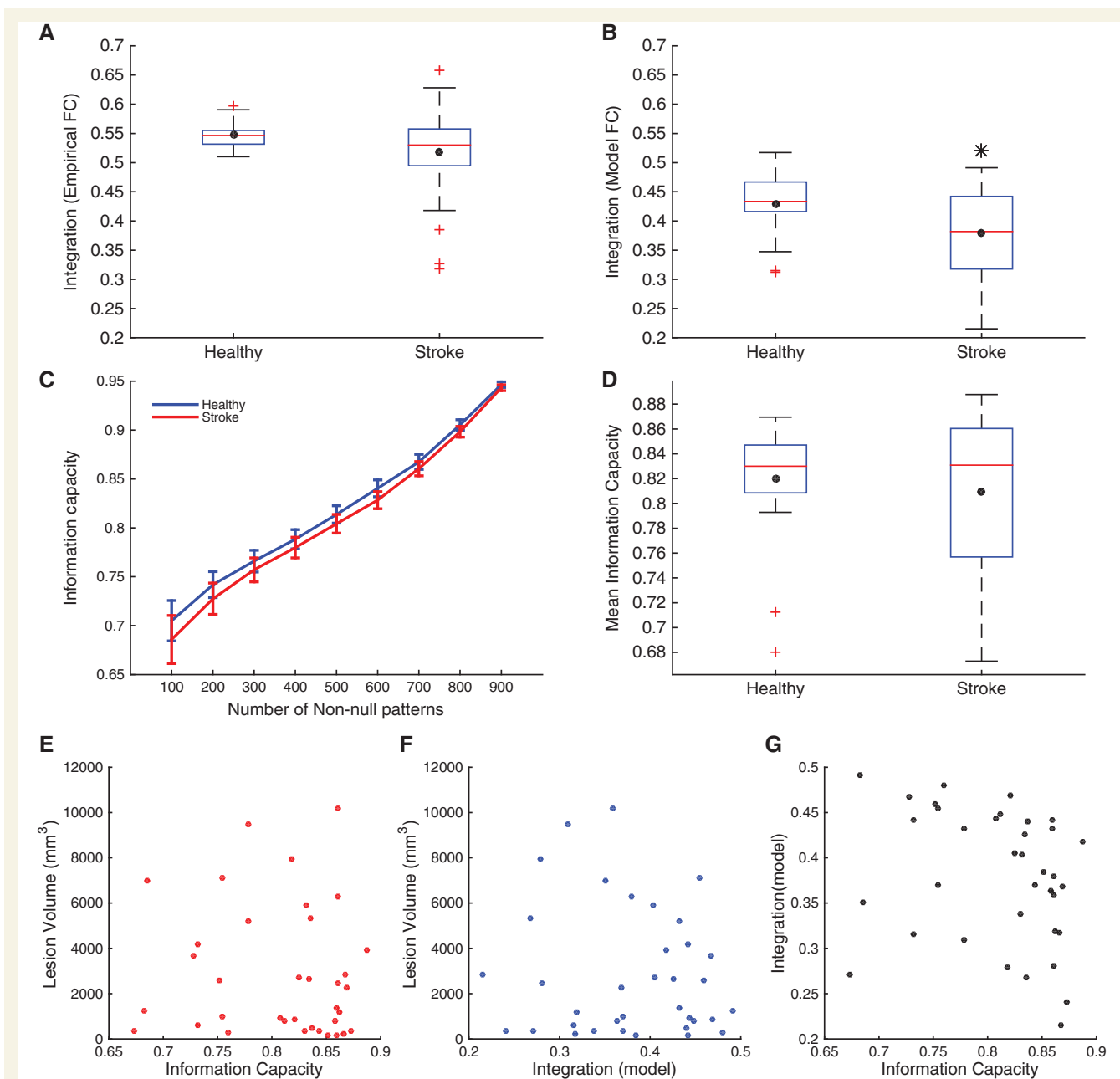


Figure 4 Integration and information capacity in controls and stroke. (A and B) Box plot of integration values calculated using the empirical functional connectivities (A) and model functional connectivities (B) of all healthy subjects and stroke patients. (C) Mean information capacity (\pm standard error of the mean), averaged across healthy control subjects (blue) and stroke subjects (red) for nine different numbers of non-null patterns (i.e. the activity of at least one brain area is above a threshold). For this comparison, we determine the threshold for each subject to obtain identical number of non-null patterns which are used to calculate the entropy for each subject. (D) Box plot of information capacity, averaged across values for nine different numbers of non-null patterns, of all healthy subjects and stroke patients. The black dot in each box plot indicates the mean while the red line indicates the median. The black asterisk indicates a significant difference in the group averages ($P < 0.05$, unpaired t -test). (E and F) Lack of correlation between values of total lesion volume and information capacity (E) and model integration (F) demonstrate that the values for these two measures are not a direct consequence of total structural damage. (G) Lack of correlation between values of information capacity and model integration.

common functional connectivity changes described in stroke. Specifically, homotopic interhemispheric functional connectivity correlated strongly with integration, and more limitedly with information capacity; abnormal correlation between

RSNs in the damaged hemisphere was clearly related to information capacity not integration. Finally, both integration and segregation measures related to behavioural impairment across subjects.

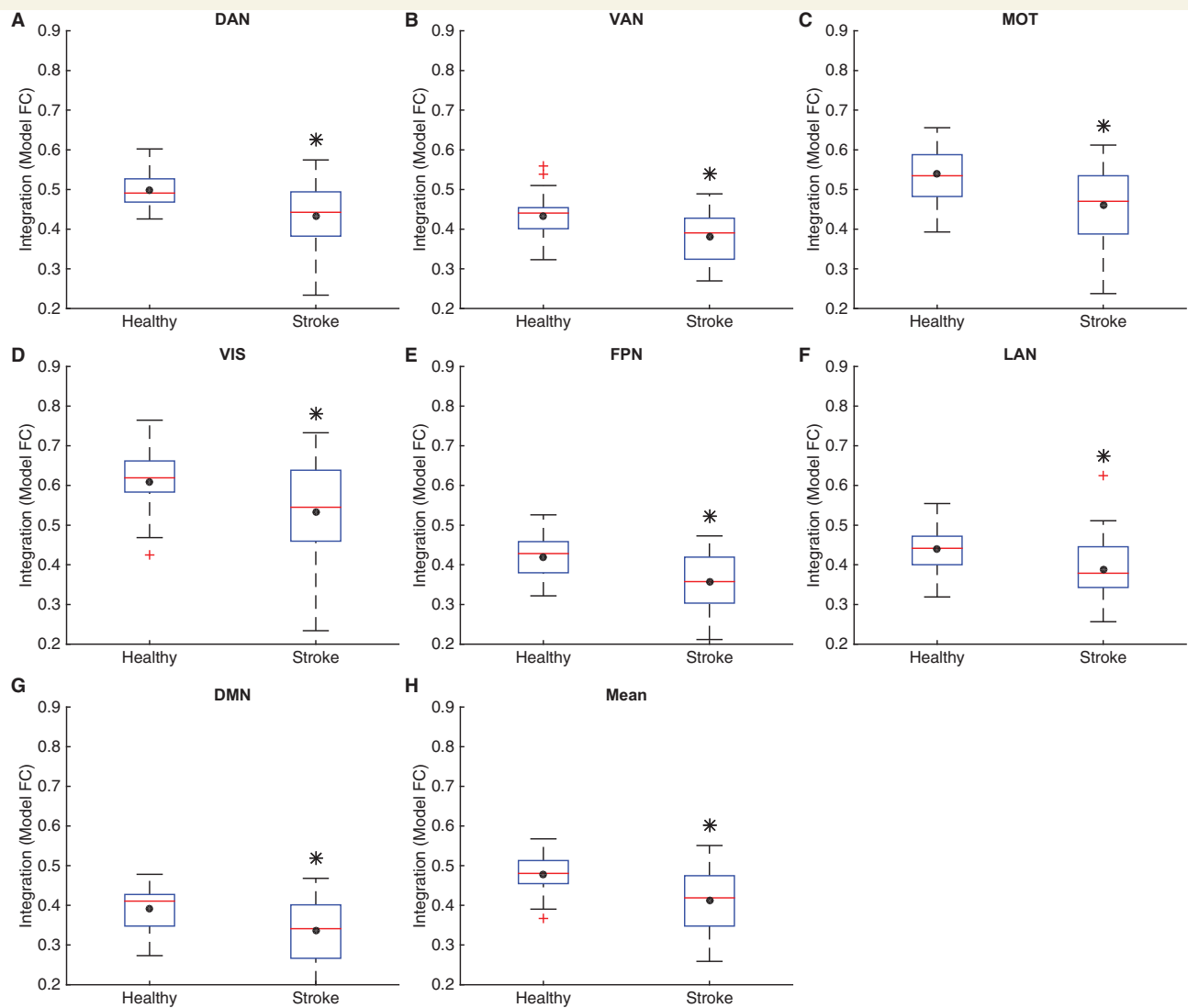
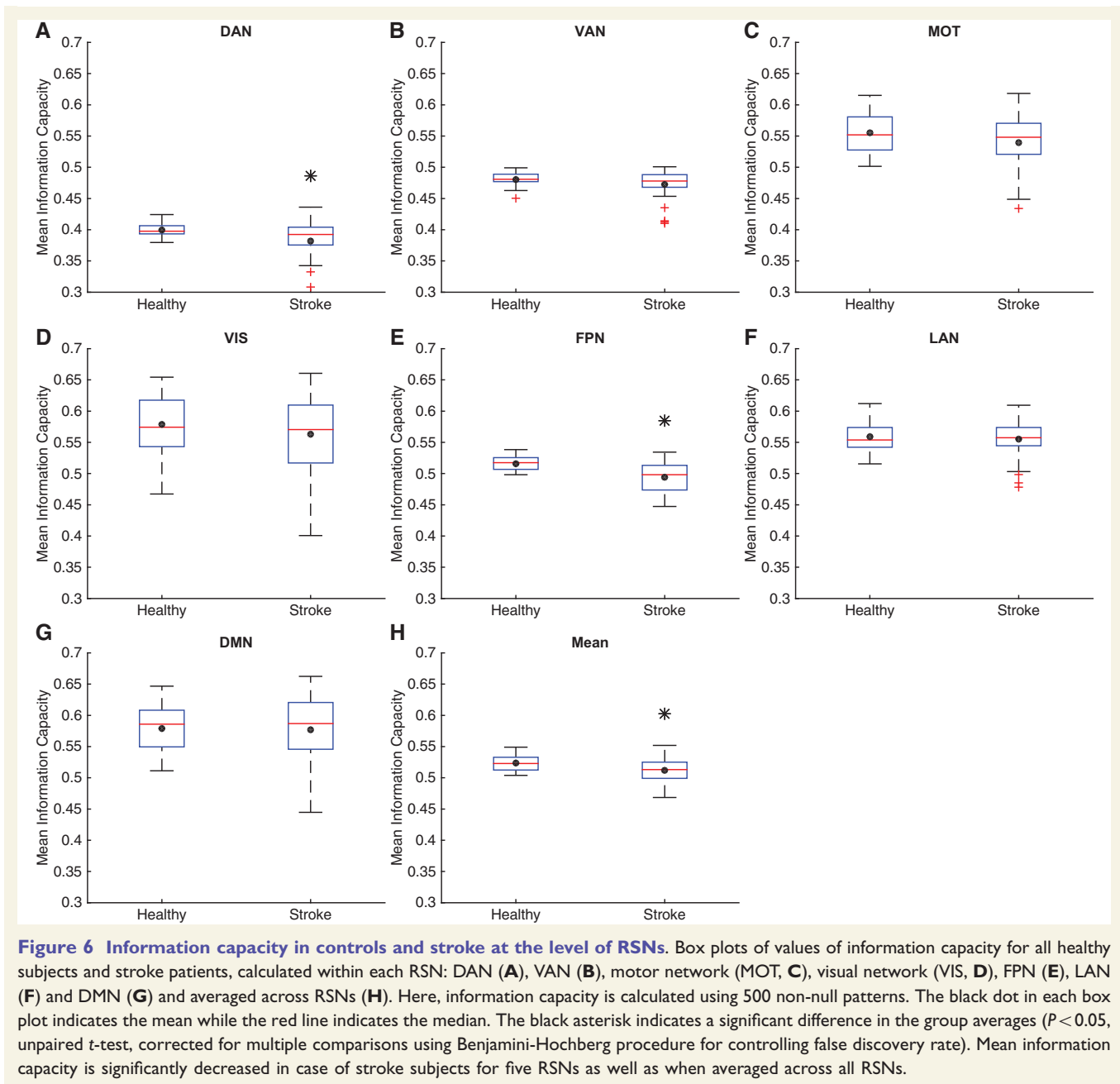


Figure 5 Integration in controls and stroke at the level of RSNs. Box plots of values of integration for all healthy subjects and stroke patients, calculated within each RSN: DAN (A), VAN (B), motor network (MOT, C), visual network (VIS, D), FPN (E), LAN (F) and DMN (G) and averaged across RSNs (H). The black dot in each box plot indicates the mean while the red line indicates the median. The black asterisk indicates a significant difference in the group averages ($P < 0.05$, unpaired t -test, corrected for multiple comparisons using Benjamini-Hochberg procedure for controlling false discovery rate). Mean integration is significantly decreased in case of stroke subjects for all RSNs as well as when averaged across RSNs.

Computational modelling of stroke

Our computational approach is based on the premise that it is possible to create a model of whole-brain connectivity in an individual injured brain. The network model couples mean field models for local regions via a structural connectome, averaged across 10 healthy subjects, and is optimized for each healthy and stroke subject using individual empirical functional connectivity. Optimization derives an effective connectivity by adjusting the synaptic weight of all inter-hemispheric connections and all other connections stronger than 0.5% of the strongest connection in the original structural connectivity matrix. The optimization leads to very similar (correlation wise) model and empirical functional connectivity matrices, $r \sim 0.75$ (Fig. 3G).

The rationale behind considering all interhemispheric homotopic connections (whether existing originally or not) in the optimization procedure lies in the limitation of the diffusion spectrum imaging methods in identifying interhemispheric tracts that traverse the corpus callosum. These are important connections that are found in the functional connectivity of healthy individuals and are regularly missed in the structural connectome obtained by DTI/DSI. In non-human primates, these structural connections have been directly found in tracing studies. Further, diminished functional connectivity between interhemispheric homotopic regions is a robust measure found in stroke subjects (Baldassarre *et al.*, 2014; Siegel *et al.*, 2016); therefore it was important to accurately characterize these connections in the model functional connectivity.



One limitation of this approach is the possibility of over-fitting due to optimization of several scaling parameters. Limited number of data points (functional MRI scans per subject) available also limit the robustness of the estimation procedure given the number of free parameters (18% of total connections). However, using a single scaling parameter as used in previous studies (Deco *et al.*, 2013; Adhikari *et al.*, 2015) yields a significantly lower fit between model and empirical functional connectivity, maximum $r = \sim 0.45$ (Supplementary Fig. 8). Also, when we trained the effective connectivity algorithm using part of the data we found that the correlation between the trained model functional connectivity and empirical functional connectivity from the

other part of the data, did not differ much from that in the training phase (Supplementary Fig. 3). Third, given diffusion spectrum imaging has its own limitations in correctly estimating structural connectivity (particularly for inter-hemispheric pathways), and the difficulty of estimating tractography in stroke subjects, this strategy seems a sensible compromise as proof-of-concept of whole brain computational modelling in stroke.

Another limitation is that we cannot directly estimate the effect of the structural lesion on the model functional connectivity; in other words, we cannot relate for instance lesion topography or volume to specific topographic changes in model functional connectivity, or separate the

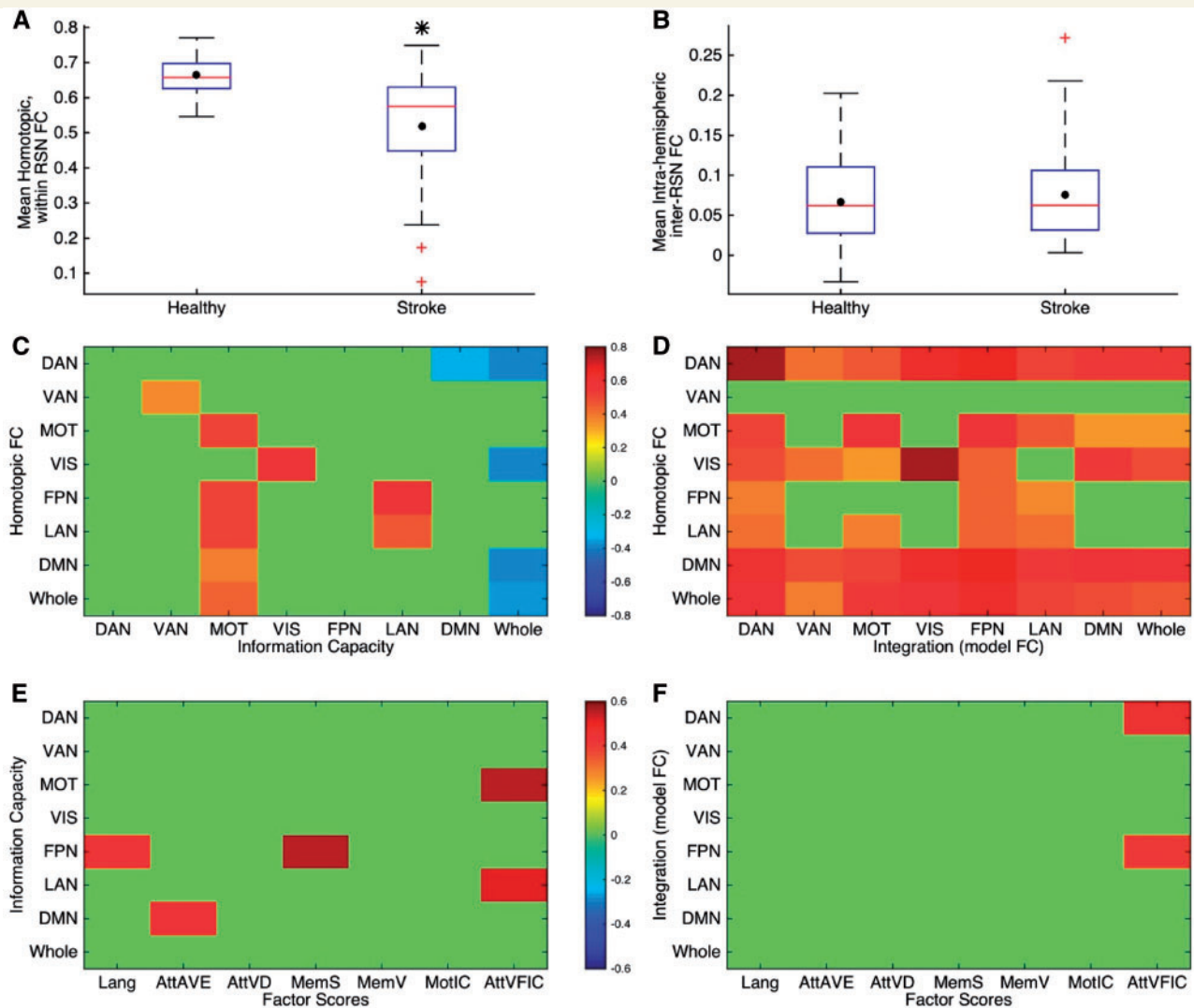


Figure 7 Relationship between computational measures and functional connectivity-based and behavioural measures.

(A and B) Box plots of values of (A) average functional connectivity (FC) between all homotopic areas within each RSN, averaged across RSNs and (B) average inter-RSN [between DAN, VAN, motor network (MOT), visual network (VIS) and DMN, FPN, LAN], intrahemispheric (ipsilesional hemisphere for stroke participants) functional connectivity. The black dot in each box plot indicates the mean while the red line indicates the median. The black asterisk indicates a significant difference in the group averages (here, $P = 0.001$, unpaired t -test). (C and D) Correlation between values of information capacity (C) and model integration (D) for stroke participants with the corresponding average interhemispheric functional connectivity between homotopic areas within each RSN and for the whole brain network. Here all non-zero values are the only correlations which were found to be significant ($P < 0.05$, calculated using a permutation test, not corrected for multiple comparisons). When corrected for multiple comparisons using Benjamini-Hochberg procedure for controlling false discovery rate, homotopic functional connectivity within most RSNs except the VAN correlates significantly at 0.05 level with the corresponding model integration while homotopic functional connectivity in motor, FPN and LAN is found to display significant correlation with motor information capacity values. (E and F) Correlation between values of information capacity (E) and model integration (F) within each RSN and for the whole brain network with behavioural factor scores obtained from within domain factor analyses for all participants with stroke. Here all non-zero values are the only correlations which were found to be significant ($P < 0.05$, calculated using a permutation test, not corrected for multiple comparisons).

effects of direct anatomical disconnection from transynaptic physiological effects. An improvement of this computational approach will require obtaining accurate structural connectivity information for each stroke subject. However, although the structural lesion was not used to directly ‘damage’ the model structural connectivity, differences in effective connectivity between healthy and stroke subjects

are related to the actual damage of different cortical regions (Fig. 3H). This result gives confidence that the optimized model functional connectivity is indeed related to the lesion.

A caveat to the interpretation of our study arises from unequal sampling of lesions across the cortex. Our sample of cortical lesions was taken from a stroke dataset shown

to represent the much larger clinical sample of stroke. These included anterior cerebral artery (3/36), middle cerebral artery (21/36), and posterior cerebral artery (12/36). The somewhat higher incidence of posterior cerebral artery strokes likely arises from the cortical stroke selection criterion.

The most important advantage of a whole brain computational model of stroke is the ability to estimate measures of information processing that are not obtainable in patients. While a graph theoretical measure like integration can be derived from empirical functional connectivity, information capacity is a purely model based measure that cannot be obtained experimentally unless to submit a patient to thousands of different stimuli and tasks. A network model optimized to represent empirically observed resting state functional connectivity allows exploration of its responses to a wide range of distinct stimuli or tasks, effectively exploring the possible range of neural states that a brain can generate. This approach is theoretically supported by the empirical observation that indeed resting state patterns of activity constrain in space and time task patterns. In fact the topography of resting state patterns is similar to that observed during task behaviour (Smith *et al.*, 2009; Cole *et al.*, 2014), and that task states are subtle but consistent modulations of resting states (Betti *et al.*, 2013; Spadone *et al.*, 2015):

A limitation of the current approach is that the randomly generated stimuli do not resemble any specific task-like conditions. The network model represents the empirically observed RSNs when it is in a stationary regime. Therefore, we apply a constant external current to the local excitatory neuronal population of each of the randomly chosen brain regions to represent a stimulus condition; in contrast, in real task-like conditions this external input would be time-dependent. However, the information capacity measures used in this study primarily reflects the ability of the network model to encode different stimuli in distinct spatial, not temporal, patterns. Therefore, it is independent of the specific design of the stimuli as long as identical designs are used for different conditions and for all subjects.

Integration and information capacity in stroke

The first and potentially most important result from this study is that structural damage caused by stroke causes a decrease of integration and segregation of brain networks. Especially important is the observation that focal lesions produce alterations of resting dynamics that lead to a decrease of variability of task states produced by the presentation of a large number of artificial task patterns. Lesion leads to low dimensional dynamic states associated with deficits. For instance, in patients with hemiparesis post-stroke, a reduction of the variability of correlated EMG patterns during natural movements has been observed that likely relate to a decrease of variability of cortical or

spinal cord synergies of neural activity (Cheung *et al.*, 2009).

If a network is completely uncorrelated, its information capacity is a maximum while the integration is zero (as the size of a maximally connected component is 0 for any threshold). On the other hand, if the network is perfectly correlated, the information capacity is zero while the integration is maximum. Thus, conceptually these two measures would be expected to be anti-correlated with one another in extreme cases. However, the information capacity is a non-linear measure of variability of responses and so is the size of the largest connected component as a function of the threshold from which integration is calculated. Therefore, they may not display any correlation in real situations as was found for participants with stroke in this study, thereby indicating that they capture different aspects of brain function.

The loss of integration and information capacity in stroke was much stronger when measured at the level of RSNs. In the case of information capacity this can be attributed to the higher impact that a lesion can have on the variability of response of regions connected in a local network as compared to the whole brain network. Owing to the reduced dimensionality of RSNs the theoretical number of distinct non-null response patterns is diminished exponentially ($2^n - 1$; where n is the number of regions). The existence of a lesioned region within an RSN diminishes both the local activity and propagation of activity to connected regions thereby accentuating the impact on variability of responses in this already shrunken state space. A stronger difference in the average integration, between stroke patients and healthy subjects, at the level of RSNs suggests a stronger decrease in the connectedness of RSNs of stroke patients in comparison with the whole brain network. This is supported by the observation that integration more strongly correlates with homotopic within-RSN than between-RSN functional connectivity (Fig. 7). More generally our results confirm the importance of RSN as spatiotemporal structures of neural activity that organize brain dynamics both at rest and during tasks.

Relationship to empirical functional connectivity changes and behavioural deficits

Decrements of interhemispheric homotopic functional connectivity across different networks, and abnormal increases of correlation in the damaged hemisphere between networks that are normally independent or negatively correlated are emerging as the two most robust network phenotypes of stroke (He *et al.*, 2007; Carter *et al.*, 2010; Baldassarre *et al.*, 2014). Importantly, these abnormalities present at the subacute stage explains large amounts of behavioural variance, especially for cognitive deficits.

A key issue, then, for the biological plausibility and potential application of whole brain models to stroke, and

more generally other disease states, is whether model-based measures of network segregation/integration relate to empirical measures of connectivity and behaviour. Indeed, we found a robust correlation of both integration and segregation measures with empirical functional connectivity changes in stroke. There was a significant positive correlation between integration measure and homotopic functional connectivity in stroke patients at the level of several RSNs as well as the whole-brain (Fig. 7D). This clearly relates to the importance of interhemispheric connectivity in organizing RSNs as interhemispheric correlations are among the strongest connections in the brain. On the other hand, information capacity displayed a stronger correlation with abnormal intrahemispheric between-RSN functional connectivity (e.g. DAN–DMN or extrinsic–intrinsic RSNs) (Supplementary Fig. 7). This link is also very interesting as the ability to encode task-specific states relates to the specialization of specific regions in each hemisphere, while high levels of inter-hemispheric synchrony are observed in states of low information processing such as seizures, sleep, low arousal, anaesthesia, etc.

Finally, also of great interest, is that model measures significantly predicted behavioural performance in real patients. The pattern of relationship, albeit *post hoc*, is intriguing. Information capacity was related to cognitive functions like attention and spatial memory whose behavioural variance is robustly predicted by large-scale patterns of abnormal functional connectivity, but not structural information (Corbetta *et al.*, 2015). Integration measures in the DAN and FPN positively correlated with visuospatial attention performance.

Whole brain dynamic models as a strategy to test novel interventions

The ability to obtain quantitative indices of networks processing dysfunction in a computer model of a damaged brain is more than of theoretical importance. It is currently unclear what a biomarker of brain dysfunction, acutely or during recovery, should look like. Several groups are measuring a number of different advance imaging metrics [e.g. fractional anisotropy (Puig *et al.*, 2013) and interhemispheric functional connectivity (Carter *et al.*, 2010)] for risk stratification and outcome prediction, but their clinical relevance remains unclear. Moreover, the data that are emerging suggest widespread alterations of connectivity while current interventions both rehabilitative and neuro-stimulation, e.g. transcranial magnetic stimulation or transcranial direct current stimulation, are directed at modulating activity at one or a few regions. The current conceptual framework in neuro-stimulation, for instance, is the notion to increase or decrease excitability at one cortical location, or rebalance activity between the damaged and normal hemisphere. The current result suggests that perhaps a better biomarker for recovery and a potential target for treatment would be the processing abnormalities that derive from abnormal global dynamics

post-stroke. Such a strategy should also take into account recent developments aimed at understanding how activity at specific nodes, or combination of nodes, control global dynamics (Gu *et al.*, 2015).

Mechanistically, integration measure is associated with connectedness of a functional brain network (whether complete or a subnetwork like a RSN). While it reflects the strength of underlying axonal pathways within the network as is evident from a significant positive correlation with homotopic functional connectivity, the largest connected component of the functional network could include motifs with areas without direct structural connections between them but with a common area. Integration measure could therefore be useful in characterizing compensatory reorganizations of the functional networks after structural lesions due to stroke. Information capacity is associated with ability of the network to encode different topological patterns in response to different stimuli. While it is difficult to speculate the measure closest to information capacity that is accessible in humans, the information capacity, for stroke patients, was found to be anti-correlated with inter-RSN intrahemispheric functional connectivity; thus information capacity could be considered as a measure of segregation of RSNs. Here, we considered subjects with only cortical strokes; an immediate next step would be to generalize the methodology of this paper to subjects with subcortical and white matter stroke to demonstrate that measures like information capacity and integration have wider applicability. These markers can be calculated using the whole-brain model and the functional connectivity at any stage after the onset of stroke in order to assess the impact of stroke as well as recovery.

Acknowledgements

We especially thank Adrian Ponce-Alvarez and Matthieu Gilson for useful discussions that improved the manuscript.

Funding

M.H.A. and G.D. were supported by the European Research Council (ERC) advanced grant DYSTRUCTURE (No. 295129). C.D.H., J.S.S. and M.C. were supported by NIH grant (R01 NS095741-01). This study was supported in part by the Neuroimaging Informatics and Analysis Center (1P30NS098577).

Supplementary material

Supplementary material is available at *Brain* online.

References

Adhikari MH, Raja Beharelle A, Griffa A, Hagmann P, Solodkin A, McIntosh AR, et al. Computational modeling of resting-state activity

- demonstrates markers of normalcy in children with prenatal or perinatal stroke. *J Neurosci Off J Soc Neurosci* 2015; 35: 8914–24.
- Alstott J, Breakspear M, Hagmann P, Cammoun L, Sporns O. Modeling the impact of lesions in the human brain. *PLoS Comput Biol* 2009; 5: e1000408.
- Andrew James G, Lu Z-L, VanMeter JW, Sathian K, Hu XP, Butler AJ. Changes in resting state effective connectivity in the motor network following rehabilitation of upper extremity poststroke paresis. *Top Stroke Rehabil* 2009; 16: 270–81.
- Baldassarre A, Ramsey L, Hacker CL, Callejas A, Astafiev SV, Metcalf NV, et al. Large-scale changes in network interactions as a physiological signature of spatial neglect. *Brain* 2014; 137: 3267–83.
- Benjamini Y, Hochberg Y. Controlling the false discovery rate: a practical and powerful approach to multiple testing. *J R Stat Soc Ser B Methodol* 1995; 57: 289–300.
- Betti V, Penna SD, de Pasquale F, Mantini D, Marzetti L, Romani GL, et al. Natural scenes viewing alters the dynamics of functional connectivity in the human brain. *Neuron* 2013; 79: 782–97.
- Brott T, Adams HP, Olinger CP, Marler JR, Barsan WG, Biller J, et al. Measurements of acute cerebral infarction: a clinical examination scale. *Stroke J Cereb Circ* 1989; 20: 864–70.
- Bullmore E, Sporns O. Complex brain networks: graph theoretical analysis of structural and functional systems. *Nat Rev Neurosci* 2009; 10: 312.
- Cammoun L, Gigandet X, Meskaldji D, Thiran JP, Sporns O, Do KQ, et al. Mapping the human connectome at multiple scales with diffusion spectrum MRI. *J Neurosci Methods* 2012; 203: 386–97.
- Carrera E, Tononi G. Diaschisis: past, present, future. *Brain J Neurol* 2014; 137: 2408–22.
- Carter AR, Astafiev SV, Lang CE, Connor LT, Rengachary J, Strube MJ, et al. Resting interhemispheric functional magnetic resonance imaging connectivity predicts performance after stroke. *Ann Neurol* 2010; 67: 365–75.
- Carter AR, Shulman GL, Corbetta M. Why use a connectivity-based approach to study stroke and recovery of function? *NeuroImage* 2012; 62: 2271–80.
- Cheung VCK, Piron L, Agostini M, Silvoni S, Turolla A, Bizzi E. Stability of muscle synergies for voluntary actions after cortical stroke in humans. *Proc Natl Acad Sci* 2009; 106: 19563–8.
- Cole MW, Bassett DS, Power JD, Braver TS, Petersen SE. Intrinsic and task-evoked network architectures of the human brain. *Neuron* 2014; 83: 238–51.
- Corbetta M. Functional connectivity and neurological recovery. *Dev Psychobiol* 2012; 54: 239–53.
- Corbetta M, Ramsey L, Callejas A, Baldassarre A, Hacker CD, Siegel JS, et al. Common behavioral clusters and subcortical anatomy in stroke. *Neuron* 2015; 85: 927–41.
- Dale AM, Fischl B, Sereno MI. Cortical surface-based analysis: I. segmentation and surface reconstruction. *NeuroImage* 1999; 9: 179–94.
- Damoiseaux JS, Rombouts SARB, Barkhof F, Scheltens P, Stam CJ, Smith SM, et al. Consistent resting-state networks across healthy subjects. *Proc Natl Acad Sci USA* 2006; 103: 13848–53.
- Deco G, Jirsa VK. Ongoing cortical activity at rest: criticality, multistability, and ghost attractors. *J Neurosci* 2012; 32: 3366–75.
- Deco G, McIntosh AR, Shen K, Hutchison RM, Menon RS, Everling S, et al. Identification of optimal structural connectivity using functional connectivity and neural modeling. *J Neurosci* 2014a; 34: 7910–16.
- Deco G, Ponce-Alvarez A, Hagmann P, Romani GL, Mantini D, Corbetta M. How local excitation–inhibition ratio impacts the whole brain dynamics. *J Neurosci* 2014b; 34: 7886–98.
- Deco G, Ponce-Alvarez A, Mantini D, Romani GL, Hagmann P, Corbetta M. Resting-state functional connectivity emerges from structurally and dynamically shaped slow linear fluctuations. *J Neurosci* 2013; 33: 11239–52.
- Deco G, Tononi G, Boly M, Kringelbach ML. Rethinking segregation and integration: contributions of whole-brain modelling. *Nat Rev Neurosci* 2015; 16: 430–9.
- Desikan RS, Ségonne F, Fischl B, Quinn BT, Dickerson BC, Blacker D, et al. An automated labeling system for subdividing the human cerebral cortex on MRI scans into gyral based regions of interest. *NeuroImage* 2006; 31: 968–80.
- Ferrier D. The functions of the brain. G P Putnam's sons, New York, 1886.
- Fox MD, Snyder AZ, Vincent JL, Corbetta M, Essen DCV, Raichle ME. The human brain is intrinsically organized into dynamic, anticorrelated functional networks. *Proc Natl Acad Sci USA* 2005; 102: 9673–8.
- Friston KJ, Harrison L, Penny W. Dynamic causal modelling. *NeuroImage* 2003; 19: 1273–302.
- Grefkes C, Fink GR. Reorganization of cerebral networks after stroke: new insights from neuroimaging with connectivity approaches. *Brain* 2011; 134: 1264–76.
- Gu S, Pasqualetti F, Cieslak M, Telesford QK, Yu AB, Kahn AE, et al. Controllability of structural brain networks. *Nat Commun* 2015; 6: 8414.
- Hacker CD, Laumann TO, Szrama NP, Baldassarre A, Snyder AZ, Leuthardt EC, et al. Resting state network estimation in individual subjects. *NeuroImage* 2013; 82: 616–33.
- Hagmann P, Cammoun L, Gigandet X, Meuli R, Honey CJ, Wedeen VJ, et al. Mapping the structural core of human cerebral cortex. *PLoS Biol* 2008; 6: e159.
- He BJ, Snyder AZ, Vincent JL, Epstein A, Shulman GL, Corbetta M. Breakdown of functional connectivity in frontoparietal networks underlies behavioral deficits in spatial neglect. *Neuron* 2007; 53: 905–18.
- Honey CJ, Sporns O. Dynamical consequences of lesions in cortical networks. *Hum Brain Mapp* 2008; 29: 802–9.
- Kelly AMC, Uddin LQ, Biswal BB, Castellanos FX, Milham MP. Competition between functional brain networks mediates behavioral variability. *NeuroImage* 2008; 39: 527–37.
- Kötter R. Online retrieval, processing, and visualization of primate connectivity data from the CoCoMac Database. *Neuroinformatics* 2004; 2: 127–44.
- Longstreth WT, Manolio TA, Arnold A, Burke GL, Bryan N, Jungreis CA, et al. Clinical correlates of white matter findings on cranial magnetic resonance imaging of 3301 elderly people. The Cardiovascular Health Study. *Stroke* 1996; 27: 1274–82.
- Mantini D, Perrucci MG, Gratta CD, Romani GL, Corbetta M. Electrophysiological signatures of resting state networks in the human brain. *Proc Natl Acad Sci* 2007; 104: 13170–5.
- van Meer MPA, van der Marel K, Wang K, Otte WM, El Bouazati S, Roeling TAP, et al. Recovery of sensorimotor function after experimental stroke correlates with restoration of resting-state interhemispheric functional connectivity. *J Neurosci* 2010; 30: 3964–72.
- Park C, Chang WH, Ohn SH, Kim ST, Bang OY, Pascual-Leone A, et al. Longitudinal changes of resting-state functional connectivity during motor recovery after stroke. *Stroke* 2011; 42: 1357–62.
- Park H-J, Friston K. Structural and functional brain networks: from connections to cognition. *Science* 2013; 342: 1238411.
- Power JD, Barnes KA, Snyder AZ, Schlaggar BL, Petersen SE. Spurious but systematic correlations in functional connectivity MRI networks arise from subject motion. *NeuroImage* 2012; 59: 2142–54.
- Power JD, Schlaggar BL, Petersen SE. Recent progress and outstanding issues in motion correction in resting state fMRI. *NeuroImage* 2015; 105: 536–51.
- Puig J, Blasco G, Daunis-I-Estadella J, Thomalla G, Castellanos M, Figueras J, et al. Decreased corticospinal tract fractional anisotropy predicts long-term motor outcome after stroke. *Stroke J Cereb Circ* 2013; 44: 2016–18.
- Robb RA, Hanson DP. A software system for interactive and quantitative visualization of multidimensional biomedical images. *Australas Phys Eng Sci Med* 1991; 14: 9–30.
- Rowland DJ, Garbow JR, Laforest R, Snyder AZ. Registration of [18F]FDG microPET and small-animal MRI. *Nucl Med Biol* 2005; 32: 567–72.

- Satterthwaite TD, Wolf DH, Loughhead J, Ruparel K, Elliott MA, Hakonarson H, et al. Impact of in-scanner head motion on multiple measures of functional connectivity: relevance for studies of neurodevelopment in youth. *NeuroImage* 2012; 60: 623–32.
- Scoville WB, Milner B. Loss of recent memory after bilateral hippocampal lesions. *J Neurol Neurosurg Psychiatry* 1957; 20: 11–21.
- Sestieri C, Shulman GL, Corbetta M. Attention to memory and the environment: functional specialization and dynamic competition in human posterior parietal cortex. *J Neurosci* 2010; 30: 8445–56.
- Siegel JS, Ramsey LE, Snyder AZ, Metcalf NV, Chacko RV, Weinberger K, et al. Disruptions of network connectivity predict impairment in multiple behavioral domains after stroke. *Proc Natl Acad Sci* 2016; 113: E4367–76.
- Smith SM, Fox PT, Miller KL, Glahn DC, Fox PM, Mackay CE, et al. Correspondence of the brain's functional architecture during activation and rest. *Proc Natl Acad Sci USA*. 2009; 106: 13040–5.
- Spadone S, Penna SD, Sestieri C, Betti V, Tosoni A, Perrucci MG, et al. Dynamic reorganization of human resting-state networks during visuospatial attention. *Proc Natl Acad Sci* 2015; 112: 8112–17.
- Sporns O. Network attributes for segregation and integration in the human brain. *Curr Opin Neurobiol* 2013; 23: 162–71.
- Talairach J, Tournoux P. *Co-Planar Stereotaxic Atlas of the Human Brain: 3-D Proportional System: An Approach to Cerebral Imaging*. Thieme 1988.
- Tononi G, Sporns O, Edelman GM. A measure for brain complexity: relating functional segregation and integration in the nervous system. *Proc Natl Acad Sci* 1994; 91: 5033–7.
- Treves A, Panzeri S. The upward bias in measures of information derived from limited data samples. *Neural Comput* 1995; 7: 399–407.
- Van Dijk KRA, Sabuncu MR, Buckner RL. The influence of head motion on intrinsic functional connectivity MRI. *NeuroImage* 2012; 59: 431–8.
- Wang L, Yu C, Chen H, Qin W, He Y, Fan F, et al. Dynamic functional reorganization of the motor execution network after stroke. *Brain* 2010; 133: 1224–38.
- Westlake KP, Nagarajan SS. Functional connectivity in relation to motor performance and recovery after stroke. *Front Syst Neurosci* 2011; 5. <http://www.ncbi.nlm.nih.gov/pmc/articles/PMC3060711/> (13 February 2016, date last accessed).